Title

Effects of topography on in-canopy transport of gases emitted within dense forests

Journal

Quarterly Journal of the Royal Meteorological Society, 145(722)

ISSN

0035-9009

Authors

Chen, Bicheng
Chamecki, Marcelo
Katul, Gabriel G

Publication Date

2019-07-01

DOI

10.1002/qj.3546

Peer reviewed

ORIGINAL ARTICLE

Effects of topography on in-canopy transport of gases emitted within dense forests

Bicheng Chen[1] | **Marcelo Chamecki**[1] | **Gabriel G. Katul**[2]

[1]Department of Atmospheric and Oceanic Sciences, University of California, Los Angeles, California, 90095, USA

[2]Nicholas School of the Environment, Duke University, Durham, NC, 27708, USA

Correspondence
M. Chamecki, Department of Atmospheric and Oceanic Sciences, University of California, Los Angeles, California, 90095, USA
Email: chamecki@ucla.edu

Funding information

The significance of air flow within dense canopies situated on hilly terrain is not in dispute given its relevance to a plethora of applications in meteorology, wind energy, air pollution, atmospheric chemistry and ecology. While the mathematical description of such flows is complex, progress has proceeded through an interplay between experiments, mathematical modeling, and more recently large eddy simulations (LES). In this contribution, LES is used to investigate the topography-induced changes in the flow field and how these changes propagate to scalar transport within the canopy. The LES runs are conducted for a neutral atmospheric boundary layer (ABL) above a tall dense forested canopy situated on a train of 2-dimensional sinusoidal hills. The foliage distribution is specified using leaf area density measurements collected in an Amazon rain forest. A series of LES runs with increasing hill amplitude are conducted to disturb the flow from its flat-terrain state. The LES runs successfully reproduce the recirculation region and the flow-separation on the lee-side of the hill within the canopy region in agreement with prior laboratory and LES studies. Simulation results show that air parcels released inside the canopy have two preferential pathways to escape the canopy region: a "local" pathway similar to that encountered in flat terrain and an "advective" pathway near the flow separation

region. Further analysis shows that the preferential escape location over the flow-separation region leads to a "chimney" like effect that becomes amplified for air parcels releases near the forest floor. The work here demonstrates that shear-layer turbulence is the main mechanism exporting air parcels out the canopy for both pathways. However, compared to flat terrain, the mean updraft at the flow-separation induced by topography significantly shorten the in-canopy residence time for air parcels released in the lower canopy, thus, enhancing the export fraction of reactive gases.

KEYWORDS
Amazon forest, canopy air parcel escape, complex topography, Large Eddy Simulation, residence time

1 | INTRODUCTION

The exchange of scalars (e.g., water vapor, carbon dioxide, ammonia, methane, ozone, aerosols, volatile organic compounds, pheromones) between forests and the overlying atmospheric boundary layer (ABL) continues to draw significant attention given its relevance to a plethora of applications in Earth systems science, biogeochemical cycling, atmospheric chemistry and air pollution, agriculture, pest control and gene flow, ecosystem health, among others. This significance is partly exemplified by the creation of the FLUXNET program – a global network of long-term single-point scalar flux measurements based on the eddy-covariance technique (Baldocchi et al., 2001) aiming to sample various biomes and climatic conditions. The key assumption in the interpretation and upscaling of FLUXNET measurements is that momentum and scalar fluxes collected above the canopy top are constant with height (Wang and Rotach, 2010; Xu and Yi, 2013; Grant et al., 2015). For more than two decades now, it has been recognized that the presence of gentle topography can have a large impact on biosphere-atmosphere exchanges of scalars and momentum even if measurements are conducted over reasonably homogeneous forests as illustrated by early model calculations discussed elsewhere (Wilson et al., 1998). Moreover, those impacts are not random and can lead to significant biases in the interpretation of FLUXNET data (Belcher et al., 2012). The problem appears more serious in the case of reactive gases as the residence time of gases inside forests can have appreciable effects on the amounts transported out of the forest (Gerken et al., 2017).

The presence of topography is particularly problematic for dense canopies, as the large momentum absorption by the vegetation enhances the impact of the topography on the flow field and even gentle topography leads to flow separation (Finnigan and Belcher, 2004; Ross and Vosper, 2005; Poggi et al., 2008; Patton and Katul, 2009; Dupont et al., 2008; Wang and Yi, 2012). The potential impact of flow separation and the consequent recirculation zone within the canopy on the transport of gases and even particles such as seeds, pollen, or aerosols has been discussed by many authors (e.g., see Finnigan and Belcher, 2004; Katul et al., 2006; Katul and Poggi, 2010, 2012; Xu and Yi, 2013; Trakhtenbrot et al., 2014; Ross and Harman, 2015; Liu et al., 2016). However, a limited number of studies have been devoted to scalar exchanges and how they may be impacted by such recirculation zone. Using a 2D model based on first-order closure, Katul et al. (2006) found that gentle topography (sinusoidal ridges) led to significant spatial variability in fluxes of CO_2 at the canopy top when photosynthetic sinks and soil respiration sources are considered together.

Two-dimensional model runs reported by Ross (2011) using a uniform gas source within the entire canopy volume confirms the existence of enhanced fluxes in the separation region. Their results also showed that the efficiency of gas transport out of the canopy is enhanced by topography, leading to lower in-canopy concentrations when compared to flat terrain. Similar 2D simulations with several source distributions over an isolated ridge performed by Ross and Harman (2015) show that the spatial variability is larger for scalars emitted near the ground than for those emitted in the upper canopy, and that there is qualitative similarity between periodic and isolated hills. Flume experiments performed by Poggi and Katul (2007) showed that the the mean recirculation region is characterized by an intermittent flow regime with alternating positive and negative velocity in the lower canopy layer. These alternations result in a vertical scalar transport at the canopy top that follows periodic cycles of accumulation and ejection. Note that a similar effect of enhanced concentrations and fluxes are observed near forest edges over flat terrain, where the flow deceleration due to the canopy drag also produces a region of mean flow convergence (Cassiani et al., 2008; Sogachev et al., 2008; Kanani-Sühring and Raasch, 2014).

Building on these prior results, the work here further explores the effects of gentle topography on the flow and transport of gases within tall and dense forests, where the leaf area density is vertically variable. The first objective was to explore whether the statistics of turbulent velocity fluctuations reasonably follow the moving equilibrium hypothesis (Yaglom, 1979), where the local turbulent shear stress at the canopy top collapses the turbulent statistics within the canopy for all positions across the hill. A second objective is to characterize the export of these gases from the forest as the hill becomes steeper. The LES is used to characterize the flow field within and above a dense forest canopy over a train of sinusoidal hills and trajectories of air parcels moving within the canopy are recorded and used to analyze the effects of topography on gas transport. A brief description of the numerical model and simulation setup are presented in Section 2. Results of the flow adjustment and the scalar transport are presented in Section 3 and the conclusions are presented in Section 4.

2 | METHODS

The LES with an immersed boundary (IB) method is used to represent the topography, and a drag force representation is used to represent the canopy effects on the flow. The implementation of the IB method for topography is based on the approach used by Chester et al. (2007). The canopy drag force representation is based on prior work of Shaw and Schumann (1992) and utilizes the implementation proposed by Pan et al. (2014). This implementation has been shown to produce results in agreement with observations across a wide range of canopy types (e.g. Pan et al., 2015; Gerken et al., 2017; Lin et al., 2018). The resulting flow field is then used to determine Lagrangian trajectories of air parcels inside the canopy, permitting unambiguous assessment of residence times and export locations of air parcels released from sources inside the canopy. A brief description of the numerical approaches and the simulation setup are provided below.

2.1 | Large eddy simulation

The LES model solves the filtered Navier-Stokes equations:

$$\frac{\partial \widetilde{\boldsymbol{u}}}{\partial t} + \widetilde{\boldsymbol{u}} \cdot \nabla \widetilde{\boldsymbol{u}} = -\frac{1}{\rho} \nabla \widetilde{p} - \nabla \cdot \boldsymbol{\tau} + \boldsymbol{F}_d + \boldsymbol{F}_r \,, \tag{1}$$

where $\widetilde{\boldsymbol{u}}$ is the filtered velocity, $\widetilde{p}$ is the filtered modified pressure field, $\boldsymbol{\tau}$ is the subgrid-scale (SGS) momentum flux, $\boldsymbol{F}_d$ represents the drag force exerted by vegetation elements, and $\boldsymbol{F}_r$ represents the immersed boundary force. The SGS momentum flux $\boldsymbol{\tau}$ is parameterized using the Smagorinsky-Lilly model (Smagorinsky, 1963; Lilly, 1967), with the Smagorinsky coefficient determined dynamically using the Lagrangian scale-dependent dynamic model (Bou-Zeid et al., 2005). The spatial discretization of the equations combine a pseudo-spectral method in the horizontal directions and a second-order centered finite difference in the vertical direction. The horizontal boundary conditions for velocity and pressure are periodic, and the entire equation system is solved using second-order Adams-Bashforth time integration scheme.

The vegetation drag force $\boldsymbol{F}_d$ is modeled as (Pan et al., 2014)

$$\boldsymbol{F}_d = -C_d\,(a\boldsymbol{P})\cdot(|\widetilde{\boldsymbol{u}}|\widetilde{\boldsymbol{u}})\,, \tag{2}$$

where C_d is a constant drag coefficient and $\boldsymbol{P} = P_x\boldsymbol{e}_x\boldsymbol{e}_x + P_y\boldsymbol{e}_y\boldsymbol{e}_y + P_z\boldsymbol{e}_z\boldsymbol{e}_z$ is the projection coefficient tensor to project the leaf area density in each direction (x refers to the streamwise direction, y refers to the spanwise direction and z refers to the vertical direction).

The topography is represented using an IB method (Peskin, 1972) following the discrete direct forcing approach (Mittal and Iaccarino, 2005). A signed-distance function ϕ is used to separate grid points inside the fluid ($\phi > 0$) from those inside the solid ($\phi < 0$), with $\phi = 0$ being points at the fluid-ground interface. The immersed boundary force $\boldsymbol{F}_r$ only acts on the ground and interface points ($\phi \leq 0$), driving the fluid velocity to zero while maintaining the incompressibility condition. Details about the calculation of $\boldsymbol{F}_r$ are reviewed elsewhere (Chester et al., 2007).

Because the LES is not wall-resolving, a wall model is applied to parameterize the SGS stress $\boldsymbol{\tau}$ at points in the vicinity of the IB. The application of the wall model follows mostly Chester et al. (2007), but without the linear extrapolation of SGS stress inside the IB. The application of the IB method creates a discontinuity in the computed variables at the fluid-ground interface, causing unphysical oscillations in physical variables near the discontinuity point (the Gibbs phenomenon). This degrades the spectral accuracy and can not be eliminated by increasing the number of modes in the truncated series. To reduce the Gibbs phenomenon, a smoothing method proposed by Li et al. (2016) is applied. This method uses a cubic polynomial function to interpolate values inside the IB while maintaining second-order accuracy.

The trajectories of air parcels are determined "offline" by integrating

$$\frac{d\boldsymbol{x}_{p,i}}{dt} = \widetilde{\boldsymbol{u}}_i + \boldsymbol{u}_{sgs,i}\,, \tag{3}$$

where $\boldsymbol{x}_{p,i}$ is the position of the i-th parcel, $\widetilde{\boldsymbol{u}}_i$ is the resolved flow velocity at the location of the i-th parcel, and $\boldsymbol{u}_{sgs,i}$ is the SGS velocity. Following Weil et al. (2004), the SGS velocity is modeled using a Langevin equation. However, the numerical integration scheme proposed by Bailey (2016) is used, which is computationally efficient and numerically stable. This scheme was shown to eliminate occurrences of unphysical trajectories that can contaminate the scalar statistics. Because the focus is on the in-canopy transport, air parcels are only tracked inside the canopy. The release of air parcels is uniform in the horizontal directions and the residence time τ as well as the escape position $\boldsymbol{x}_e$ of each air parcel is recorded when it crosses the canopy top for the first time.

2.2 | Simulation setup

The numerical experiment is based on measurements obtained during the GoAmazon field campaign in the Brazilian Amazon rainforest (Fuentes et al., 2016). The field campaign was conducted from April 2014 to January 2015 at the

Cuieiras Biological Reserve (−2.6019° latitude, −60.2093° longitude), which is located approximately 60 km north-northwest of the city of Manaus, Brazil (Fuentes et al., 2016). The research tower is located on a plateau covered by a dense primary forest with canopy height between 30 and 40 m (Tóta et al., 2012). A 50 m-tall tower (known as K34) was instrumented with nine triaxial sonic anemometers to investigate atmospheric turbulence and chemistry within and above the forest canopy layer. The sketch of simulation setup is shown in Figure 1 and the key parameters are summarized in Table 1.

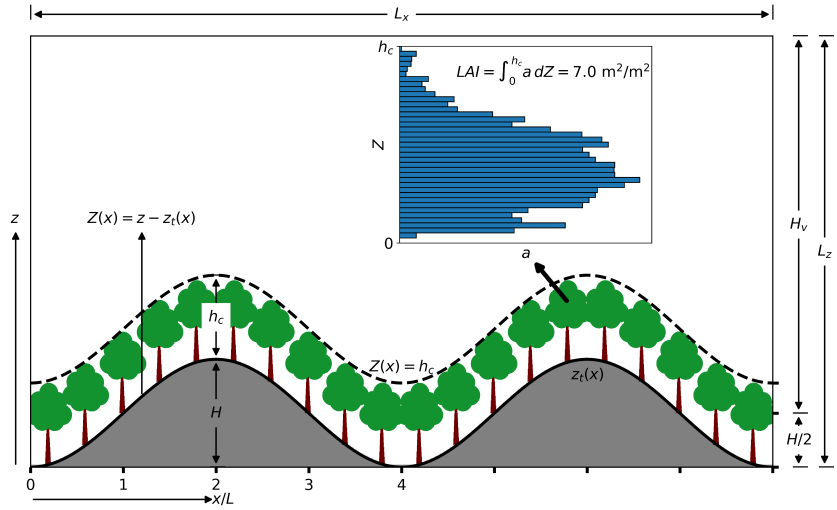

FIGURE 1 A sketch of the simulation setup. The sketch is stretched in the vertical direction from the real aspect ratio for clarity. Z is a displaced coordinate to measure vertical distance with respect to the topography.

The forest canopy is assumed to be homogeneous and continuous across the entire topography and the leaf area density profile $a(z)$ (shown as an inset in Figure 1) was based on data from Tóta et al. (2012) reported in Fuentes et al. (2016). The total leaf area index is $LAI = 7.0\ \mathrm{m^2/m^2}$ and the canopy height $h_c = 39$ m is defined based on the location where the leaf area density $a(z)$ first becomes zero. The average leaf area density throughout the entire canopy $\overline{a} = LAI/h_c$ is $0.18\ \mathrm{m^{-1}}$. The canopy drag coefficient C_d and projection tensor $\boldsymbol{P}$ follow the setup in Gerken et al. (2017), where $C_d = 0.4$ and $P_x = P_y = P_z = 1/2$, resulting in an effective drag coefficient $C_d P_i = 0.2$ ($i = x,\ y,\ z$). This estimate is in agreement with the frequently used range of $0.1 \sim 0.4$ for forests (Katul et al., 2004; Queck et al., 2011). With this value of C_d, the so-called adjustment or drag length scale can be defined as $L_c = (C_d \overline{a})^{-1} = 13.93$ m.

To permit qualitative comparisons with scalar experiments in a flume (Poggi and Katul, 2007), idealized 2D topography with shape z_t described by a cosine function is used. The topographic surface is given by

$$z_t(x) = \frac{H}{2}\cos\left(\frac{\pi}{2L}x + \pi\right) + \frac{H}{2}, \tag{4}$$

where H is the topography height, and L is the hill half length, defined as one fourth of the topography wavelength (Finnigan and Belcher, 2004). For the main simulation, labeled S0.2, the length $L = 250$ m and height $H = 50$ m are adopted as typical topography scales found in the region where the K34 tower is located (Tóta et al., 2012). The corresponding average slope is $H/L = 0.2$, and hereafter simulations are labeled based on their slope (thus, S0.2). For

TABLE 1 Key parameters of simulation setup.

Variables	Symbols	Cases			
		S0.0	S0.1	S0.2	S0.4
Horizontal domain size (m)	$L_x \times L_y$	2000×1000			
Domain height (m)	L_z	520	528	540	580
Mean air thickness (m)	H_v	515			
Grid resolution (m)	$dx \times dy \times dz$	$6.25 \times 6.25 \times 2$			
Pressure gradient acceleration (m/s^2)	$\frac{1}{\rho}\frac{\mathrm{d}p_0}{\mathrm{d}x}$	3.11×10^{-4}			
Time step (s)	dt	0.1			
Leaf area index (m$^/$m^2)	LAI	7.0			
Canopy depth (m)	h_c	39			
Canopy drag length (m)	L_c	13.93			
Ratio between canopy height and canopy drag length	h_c/L_c	2.80			
Topography height (m)	H	0	25	50	100
Topography half length (m)	L	0	250	250	250
Topography slope	H/L	0	0.1	0.2	0.4
Ratio between topography length and canopy drag length	L/L_c	17.95			

comparison, a flat terrain case labeled S0.0 is conducted. Two additional topography cases with $H = 25$ m (S0.1 with average slope 0.1) and $H = 100$ m (S0.4 with average slope 0.4) are also performed to provide a systematic investigation of the effects of hill amplitude.

Using the classification scheme proposed by Poggi et al. (2008), all the topography simulations here correspond to a deep canopy ($h_c/L_c = 2.8 > 1$) over a long hill ($L/L_c = 17.95 \gg 1$). In the deep-canopy regime, the momentum absorption by the canopy leads to flow separation and the development of a recirculation region on the lee side of the topography. In the long-hill regime, turbulence is expected to be in local equilibrium and the general framework of moving equilibrium for flows with favorable and adverse pressure gradient (Yaglom, 1979) is valid. Finally, only the S0.1 case is considered a gentle topography ($H/L = 0.1 << 1$), in the sense that the leading-order pressure perturbation is approximately fixed throughout the vertical direction so that the shape of the pressure gradients can be predicted from the topography and the outer-layer scaling (Finnigan and Belcher, 2004). The other two cases have larger H/L and fall outside the classification scheme proposed by Poggi et al. (2008).

The horizontal size of the LES domain is $L_x = 2000$ m in the streamwise direction and $L_y = 1000$ m in the spanwise direction, containing two full periods of the topography. The domain height L_z varies from 520 m to 580 m as the topography increases, while the mean thickness of the air layer (between the ground surface and domain top) $H_v = 515$ m is kept the same for all cases. The entire domain is discretized with a grid resolution of $dx = dy = 6.25$ m in horizontal directions and $dz = 2$ m in the vertical direction. With this resolution, the canopy is resolved by the first 20 layers above the ground ($dz/h_c = 0.05$). This domain size is considered large enough to represent the flow within and above the canopy under neutral conditions. Specifically, the domain height $L_z > 10h_c$ guarantees negligible effects of the top

boundary condition on turbulence statistics in the region where $Z/h_c < 2$ (Pan et al., 2014). In addition, $L_z \approx 5h_m$, where $h_m = 107.77$ m is the middle layer height implicitly defined via $(h_m/L)\ln^{1/2}(h_m/z_0) = 1$, where z_0 is the roughness length associated with the canopy (Hunt et al., 1988; Finnigan and Belcher, 2004). This guarantees that the upper portion of the domain is in the outer layer and the vertical velocity perturbation induced by the topography is close to zero.

The flow is driven by a mean pressure gradient force $\rho^{-1}\mathrm{d}p_0/\mathrm{d}x = 3.11 \times 10^{-4}$ m/s^2 in the streamwise direction. The integration of this pressure gradient force in the vertical direction is balanced by a mean frictional force associated with a friction velocity $u_* = 0.4$ m/s for the flat terrain case (hereafter termed as equivalent friction velocity). The simulations are run with neutral conditions, and the Coriolis acceleration is neglected due to the limited domain size. The integration timestep is set to $dt = 0.1$ s. The simulations are run for 4 hours of spin-up and then another 3 hours to produce flow statistics. Statistics of the flow are obtained by averaging results in space and time. Time averaging is performed over the final 3-hour period, while space averaging is performed over the y-direction and at the two x locations with the same topography phase.

Lagrangian parcels are released at 19 heights between 1 m and 37 m above the ground with 2 m interval. Their initial horizontal positions are randomly chosen from a uniform distribution. A large number of parcels (5.13×10^7) is evenly released during the 3-hour simulation. The velocity output from the LES is linearly interpolated when integrating the parcel trajectories.

3 | RESULTS

3.1 | Flow field and the moving equilibrium hypothesis

For comparison with the field measurements, LES results have been transformed into a local coordinate system with streamwise component along the topography and the vertical component perpendicular to the topography. This coordinate system is appropriate because we are only interested in the flow inside and just above the canopy. In the context of this work, we interpret the moving equilibrium hypothesis first proposed by Yaglom (1979) according to Katul et al. (1999): if we assume that the non-homogeneity imposed by the local pressure gradients produced by the topography are a slow varying function of x and y, then the local friction velocity at the canopy top $u_{*,L}(x, y)$ can be considered as a local scaling velocity, and the local turbulence statistics scaled by the $u_{*,L}(x, y)$ become independent of horizontal position. To assess the moving equilibrium hypothesis, the local friction velocity at the canopy top $u_{*,L}$ is used as a normalizing variable. It is to be noted that the local friction velocity varies by about 17% within the domain for the S0.2 case. The velocity profiles from the LES results are shown in Figure 2 and provide support for the moving equilibrium hypothesis: within the canopy layer, even though the mean flow is changing considerably across the hill, the second and third order moments are reasonably collapsed when normalized by the local (or positional) friction velocity (with exception of Sk_u in the lower half of the canopy, which does seem to vary with position along the topography). Gerken et al. (2017) used the height at which $Sk_u = 0$ as an estimate of the penetration depth of the shear-layer eddies. This criterion suggests that the topography enhances/reduces penetration depths of shear layer eddies on the lee/wind side of the ridge. These turbulent flow statistics profiles agree with the field measurements and, surprisingly, with their flat terrain counterpart and as well. Likewise, the relative significances of ejections and sweeps on momentum transfer from this simulation agree with those over flat terrain and field measurements. We note that these conclusions also hold for the S0.1 case, but deviations are quite significant for the S0.4 (not shown). Flume experiments for flow over hilly terrain in the presence and absence of canopies suggest that the moving equilibrium hypothesis appears to be valid in the presence of a canopy but not for the bare surface case (Poggi et al., 2007).

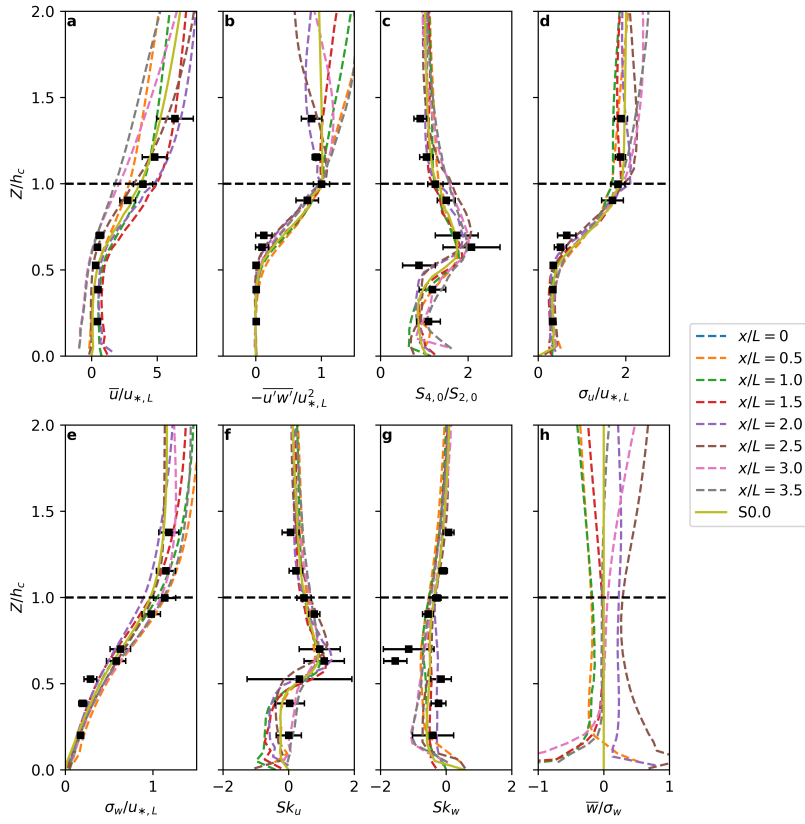

FIGURE 2 Profiles of (a) the mean streamwise velocity , (b) the mean vertical Reynolds stress, (c) the ratio of sweep to ejections for momentum fluxes, (d) the standard deviation of the streamwise velocity, (e) the standard deviation of the vertical velocity, (f) the skewness of the streamwise velocity, (g) the skewness of the vertical velocity, and (h) the ratio of the mean velocity to the standard deviation of vertical velocity. The black squares with error bars represent the K34 tower 30-min averaged measurements selected for neutrally stratified flow conditions; the solid lines represent the flat LES case and the dashed lines represent the S0.2 case. Z denotes the elevation above the ground surface and $u_{*,L}$ is the local friction velocity at the canopy top.

The mean flow streamlines and the turbulence intensity in w $\sigma_w/\overline{u}$ are shown in Figure 3. In the flat case, the mean flow streamlines are parallel to the ground and the flow is homogeneous in streamwise direction. For the cases with topography, the mean flow separates at about $x/L = 2.5$ (hereafter termed as flow-separation point) for all three cases and a recirculation zone is formed on the lee-side of the ridge. The vertical extension of this recirculation region increases as the topography height increases and finally the reversed flow extends to the top of the canopy in the S0.4 case ($H/L = 0.4$). This finding is consistent with the conclusion from Belcher et al. (2012), which reported that for small L_c/L the theory for hills with rough surfaces developed by Wood (1995) is applicable and predicts large-scale separation extending into the free air for $H/L > 0.25$.

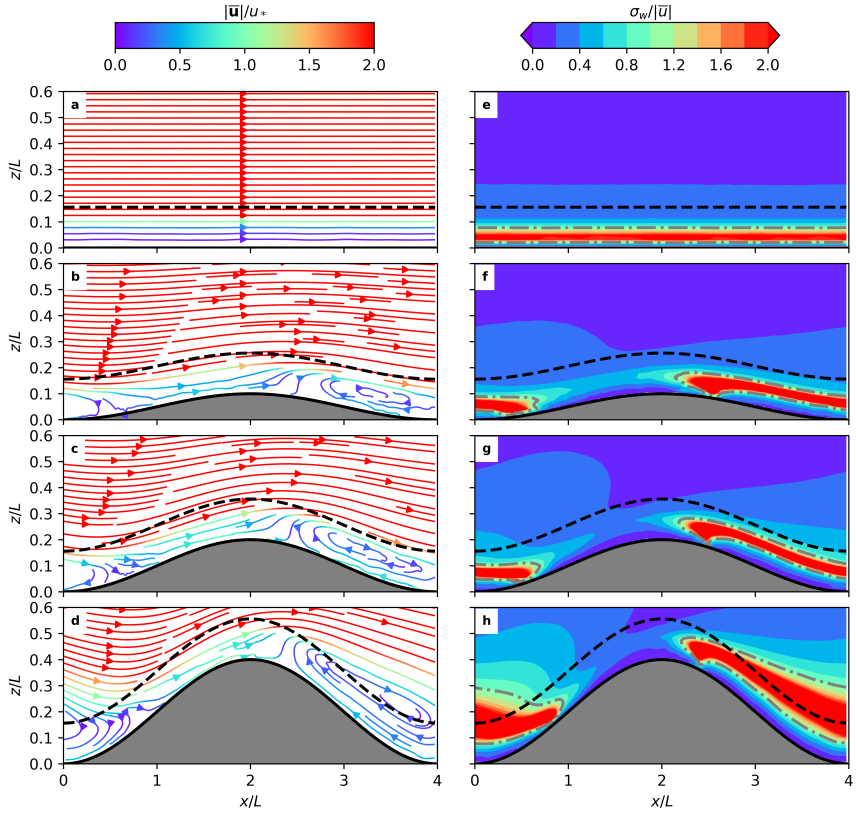

FIGURE 3 Mean flow streamlines (left) and the turbulence intensity in w (right) displayed on an $x-z$ plane. The topography height increases from top to bottom. The black dashed lines mark the position of canopy top and the gray dashed-dotted lines are isolines where $\sigma_w/\overline{u} = 1$.

The turbulence intensity in w is routinely used for diagnosing competition between mean advection and vertical turbulent transport within the canopy. For the flat case used as a reference here, the turbulence intensity in w exhibits a maximum in the lower canopy. This maximum can be understood by inspection of the profiles of σ_w and $\overline{u}$ in Figure 2. The mean velocity decays fast in the upper canopy due to the large momentum absorption resulting in a decrease of momentum transport from above, but it reaches a region of little variation with z in the lower canopy where the flow

is produced by a balance between the pressure gradient force and the canopy drag. In the upper canopy most of the turbulence is produced by shear, while in the lower canopy turbulence driven by pressure perturbations above the canopy becomes dominant (Shaw and Zhang, 1992). These features lead to a maximum in the turbulence intensity in w in the lower canopy. For cases with topography, the pattern of turbulence intensity in w is more complicated. Because the profiles of vertical velocity variance within the canopy do not change much with location (Figure 2e; note that $u_{*,L}$ only varies by 17%), most of the variation seen in Figure 3fgh is caused by changes in the mean velocity. In particular, regions with low mean streamwise velocity such as the separation region, the reattachment region, and the center of the recirculation zone have very large turbulence intensity in w. These results aid in the interpretation of air parcel trajectories discussed next.

3.2 | The two pathways for in-canopy scalar transport

When each Lagrangian parcel first cross the canopy top, its position x_e along the topography direction is recorded (the escape location). Figure 4 shows the probability density function (PDF) of x_e for the three topography cases as a function of release height inside the canopy. Parcel release is uniformly distributed in the direction along the topography. A clear preferential escape location near the flow separation point ($x/L \sim 2.5$) is evident for all three topography cases. The flow separation region appears to behave as a "forest chimney". This effect is present for sources at all heights within the canopy, becoming more dominant for sources near the canopy bottom. For parcel release near the ground, the peak of the PDF at the chimney can be more than an order of magnitude larger than that for flat terrain. The existence of these chimneys has been suggested by the analytical model of Finnigan and Belcher (2004) and later confirmed by flume experiments (Poggi and Katul, 2007, 2008), LES studies (Dupont et al., 2008; Patton and Katul, 2009) and Reynolds-averaged closure model runs (Katul et al., 2006; Ross, 2011).

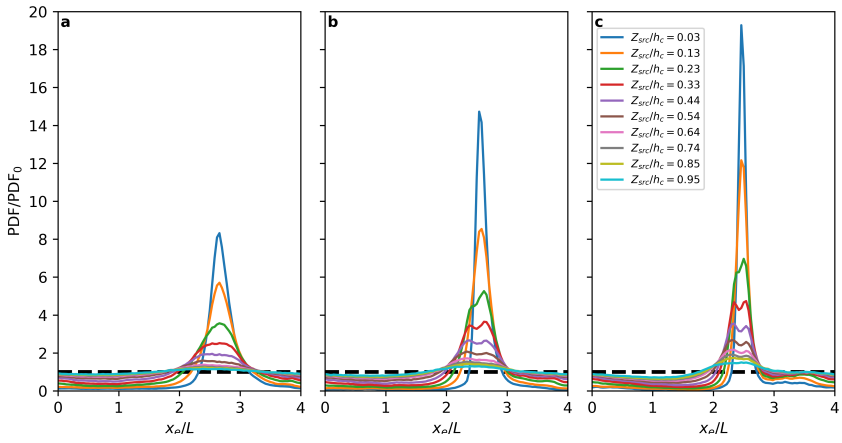

FIGURE 4 Probability density function (PDF) of escape location for sources set at several release heights within the canopy. Results shown for (a) S0.1, (b) S0.2, and (c) S0.4 cases. Here Z_{src} is the source height above the topography. All PDFs are normalized by the uniform PDF corresponding to the flat terrain simulation S0.0 (indicated as PDF_0). The thick black dashed line at $PDF/PDF_0 = 1.0$ indicates no deviations from the flat terrain case (S0.0).

To explore how parcels released at different locations contribute to the chimney effect, the canopy layer was divided into a 2 m × 2 m cartesian grid on the x–z plane. The PDF of escape locations of parcels released within each grid

box were then calculated. The modes of these PDFs (the maximal values of the PDFs) for all four simulations are shown in Figure 5. In this figure, the position of preferential escape for parcels released at any location within the canopy can be inferred by following the different colored areas. The interpretation for the flat case is straightforward: parcels are transported vertically by turbulence and advected downwind (to the right) by the mean flow. Thus, parcels escape the canopy to the right of their release position, with the streamwise distance increasing as the source approaches the ground. This leads to the tilted patterns seen in Figure 5(a). The mode of the PDF for parcels released near the ground can be displaced approximately $0.5L = 125$ m $\approx 3h_c$ from their release location (obviously individual parcels may travel much farther). In this case, a horizontally uniform release implies a horizontally uniform escape, as already shown in Figure 4.

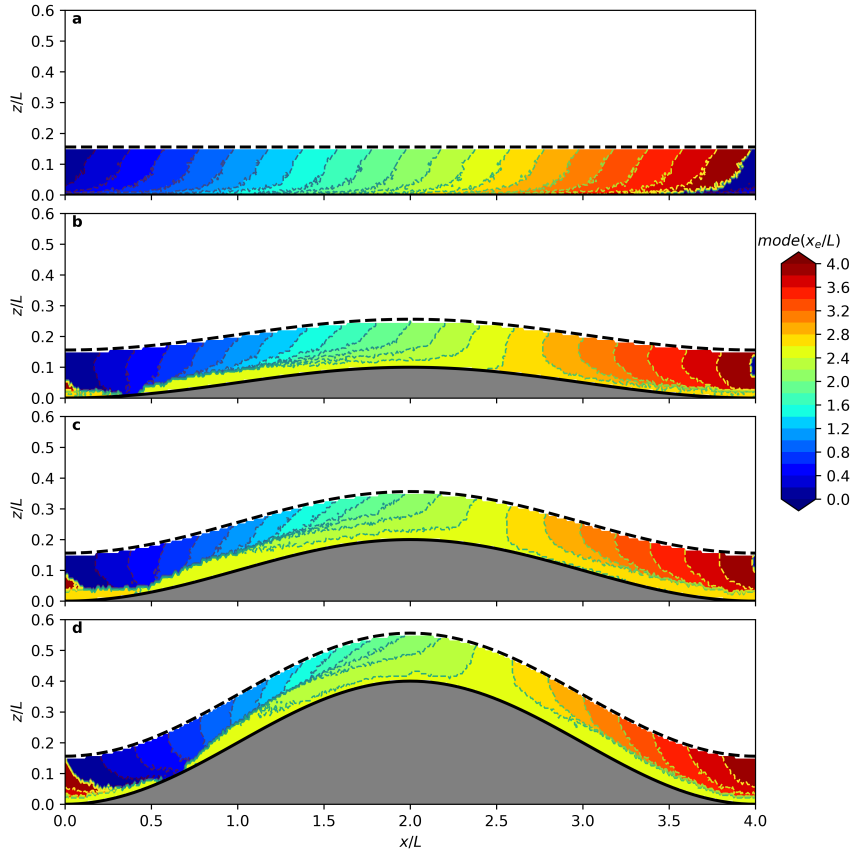

FIGURE 5 Mode of the probability distribution of escape location at the canopy top for (a) S0.0, (b) S0.1, (c) S0.2 and (d) S0.4 topographies. The dashed lines are isocontours with interval of 0.2 in x_e/L.

In the presence of topography, the emerging picture for scalar transport is quite different. Not only the flow reversal in the recirculation zone changes the direction of the advection, but also a clear separation between different escape locations emerge in the deep canopy. The juxtaposition of distant colors (e.g. dark blue and yellow) suggests that a small displacement in the source location can be enough to switch the mode of the PDF from escaping the canopy "near" the source location to escaping the canopy at the chimney location (i.e. near the separation point). The overall area within

the canopy with the mode escaping through the chimney is also amplified as the topography height increases, due to an increase in the size and strength of the recirculation. Perhaps more importantly, this result shows that a significant portion of the parcels that escape through the chimney are actually released far from the chimney location.

The sharp transition between these two modes can be explained by inspecting the entire PDFs of escape location (and not just the mode, as shown in Figure 5). For this analysis, we select one windward source position ($x/L = 1$) and one leeward source position ($x/L = 3.5$) as examples, and display the PDFs of escape location for several release heights in the simulations S0.4 and S0.0 in Figure 6 (for flat we only display PDFs for $x/L = 1$, since the flow is horizontally homogeneous). For the flat case, all the PDFs have one single mode followed by an exponential decay (note the logarithmic scale on the y-axis). The mode is typically located close to the source. Only releases close to the bottom layers of the canopy display a significant downwind shift in the mode (of about $0.5L$, as previously noted). The horizontal proximity between source and peak in the PDF of the escape locations is indicative that parcels are transported out of the canopy fairly quickly, suggesting the dominance of large coherent eddies capable of exporting parcels in few eddy turnover times (i.e. a dominance of transport by strong ejection events). This finding appears to be reasonable for the upper 2/3 of the canopy, when a shift in behavior becomes noticeable (this is also visible in the slopes of the isocontours in Figure 5(a)).

The PDFs for the S0.4 case are quite different and revealing: all release heights at both locations display a bimodal distribution of escape position confirming the existence of two distinct pathways for parcel escape: (1) the "local pathway" represented by the peak near the source corresponding to air parcels that are transported out of the canopy by strong ejection events, and (2) the "advection pathway" represented by the peak at the separation point corresponding to air parcels that travel with the recirculating flow until they reach the separation point before being transported out of the canopy. The position of the two peaks does not change much with release height, and the predominance of one peak over the other is determined by the competition between vertical turbulent transport and horizontal advection. Most air parcels released near the canopy top are quickly transported out of the canopy by vertical turbulent eddies, as clearly seen by the strong predominance of the local pathway in the PDFs in Figure 6(c). As the source is moved deeper into the canopy, the time needed for turbulent transport increases and the likelihood of air parcel to follow the advection pathway increases. The smooth transition between the dominance of one pathway over the other appears as a sharp transition in Figure 5. The dominance of the advection pathway, which is illustrated by the yellow and orange areas near the ground in Figure 5(b)-(d), corresponds approximately to the area of small $\sigma_w/|\overline{u}|$ in Figure 3(f)-(h). The parcels that follow this pathway are initially transported along the topography direction until they reach the location of the separation point where, due to flow convergence, no mean horizontal advection takes place. Except at the bottom of the canopy, the mean vertical velocity caused by the flow convergence is quite small compared to the vertical velocity fluctuations produced by the passage of large eddies (see brown line in Figure 2(h)). Thus, the parcels that arrive at the flow separation point are slowly transport upwards by the weak mean vertical velocity, until they are caught by a strong ejection event that quickly transports them out of the canopy. Thus, most of the transport is still performed by turbulent motions, even though the mean vertical velocity adds an important positive vertical drift that lifts parcels from a weak turbulent zone to an elevated and energetic turbulent zone. This predominance of transport by ejection motions at the separation point is consistent with the flume observations by Poggi and Katul (2007) showing a sequence of accumulation-ejection cycles for scalar transport at this location. The existence of these two pathways and the dynamics of the transport described here are clearly seen in the flow visualization included in the Supporting Information (see Video S1).

To gain further insight into the PDFs described above, we build an idealized model to represent the escape of parcels from the canopy. Consider a cloud of marked air parcels that is "released" at a source location with a parcel concentration C_0. This cloud is transported horizontally by the mean flow within the canopy, while interacting with eddies that remove a

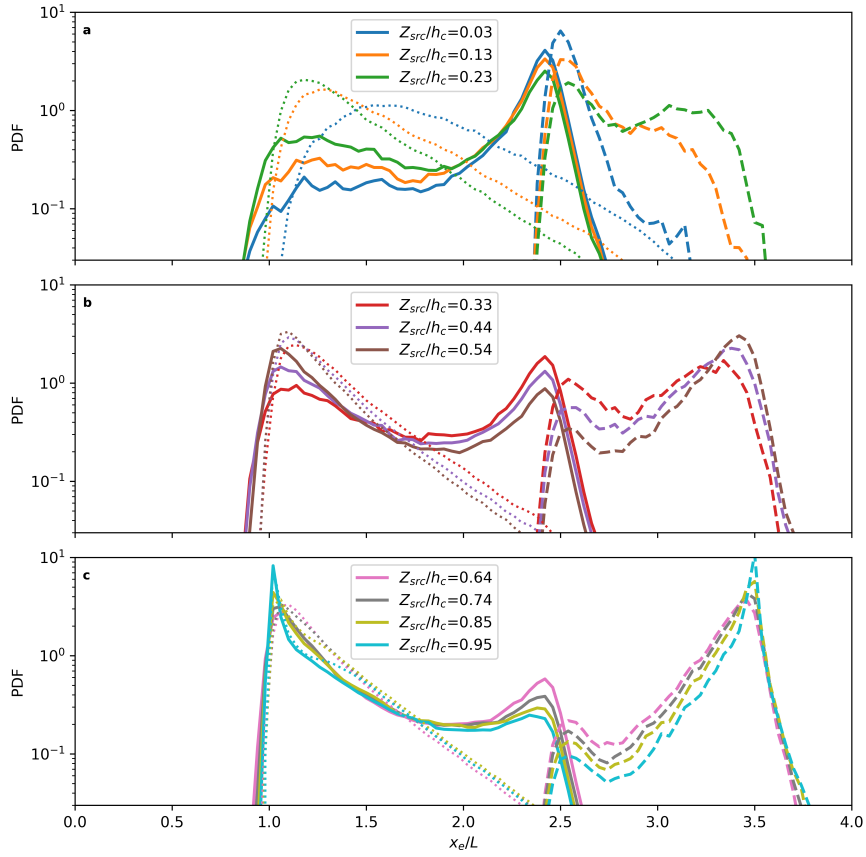

FIGURE 6 Probability density function (PDF) of escape locations for air parcels released at $x_e/L = 1$ (solid lines for S0.4 and dotted lines for S0.0) and $x_e/L = 3.5$ (dashed lines for S0.4) at (a) $Z_{src}/h_c \leq 0.23$, (b) $0.33 \leq Z_{src}/h_c \leq 0.54$ and (c) $Z_{src}/h_c \geq 0.64$.

fraction of the total remaining parcels $C(t)$ (with some efficiency time scale f_e^{-1}). These parcels are instantly transported out of the canopy. In this model, the escape as a function of time is proportional to $C(t) = C_0 \exp(-f_e t)$. By considering the mean advection velocity U, one can infer that the distribution of escape fraction as a function of distance from the source is proportional to $C(x) = C_0 \exp[-(f_e/U)x]$. Thus, the length scale $\ell_e = (f_e/U)^{-1}$ in the exponential decay of the escape fraction as a function of distance form the source is proportional to the advection velocity (i.e. large mean velocity implies a slower decay of the distribution with distance from the source). This behavior is depicted as a red line in the conceptual model for the PDF of parcel escape depicted in Figure 7.

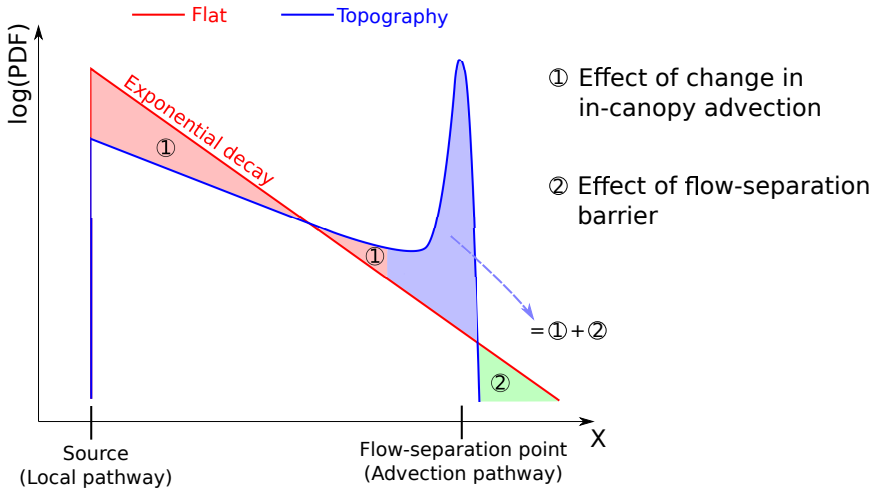

FIGURE 7 Conceptual model illustrating the bimodal PDF of parcel escape produced by the existence of two pathways: the local pathway representing escape near the source and the advection pathway representing escape near the separation point.

The modification of the PDF due to the presence of topography is caused by two distinct processes. Firstly, the presence of topography modifies the mean advection velocities within the canopy. As seen in the streamlines in Figure 3, velocities near the ground tend to be larger in the case with topography. As noted above, this implies a slower exponential decay of the PDF with distance from the source, as depicted by the blue line in Figure 7. The second modification is that now the advection distance is bounded by the separation point. Once the plume reaches the separation point, advection along the topography ceases and all remaining parcels eventually escape at the separation location, generating the second peak illustrated in Figure 7. The distance between the two peaks is approximately the distance between the source and the separation point. These two changes (corresponding to areas 1 and 2 in the figure, respectively) determine the proportion of the air parcels that escape via the advection pathway.

3.3 | In-canopy residence time and export fraction

To assess the effects of the in-canopy transport on potential chemical loss of reactive compounds emitted from forests, the residence times of the air parcels is now calculated. The median residence times for all LES runs are shown in Figure 8a. As expected from the results in the previous section, only air parcels released in the bottom 1/3 of the canopy have their residence times significantly impacted by topography. Despite the longer transport distance traveled by air parcels near the ground in the presence of topography, residence times are significantly reduced compared to the flat

case. Moreover, little difference between the three topography cases are observed in the calculations here (S0.1 has slightly larger residence times in the lower canopy when compared to S0.2 and S0.3). Given that most of the vertical transport is carried by the turbulent fluctuations and that turbulence does not change much between the different cases, the only possible explanation for the large reduction observed from the flat case to any of the topography cases is the mean vertical advection at the flow separation point (see brown line in Figure 2(h)). Note that for air parcels close to the ground in the flat terrain (either released near the ground or transported near the ground by sweeping motions), vertical turbulent transport is slow due to a weak vertical velocity fluctuations. In the cases with topography, these air parcels are quickly transported to the flow separation point where they are lifted by the mean vertical velocity to heights where turbulence is much more energetic. Thus, the mean vertical advection within the chimney reduces significantly the residence time for these air parcels by simply lifting the parcels from zones of weak turbulence.

To further investigate the potential impacts of these changes in residence time on export fraction of reactive compounds, we used the approach employed by Gerken et al. (2017) assuming first-order kinetics. For an air parcel that spends a residence time τ inside the canopy, the export fraction of a reactive compound with chemical lifetime τ_{chem} is given by $EF = \exp(-\tau/\tau_{\text{chem}})$. The total export fraction for a compound released at a fixed height inside the canopy can be obtained by integrating the PDF of residence times multiplied by the exponential decay (see Gerken et al., 2017, for details). The results are shown in terms of a Damköhler number $Da = \tau_{\text{turb}}/\tau_{\text{chem}}$ in Figure 8b, where the turbulence time scale is simply defined as $\tau_{\text{turb}} = h_c/u_*$. Topography increases the total export fractions of reactive gases emitted in the lower canopy, and this increase can be large for specific cases (e.g. for $Da = 10^{-1}$, topography increases the export fraction from about 10% to 30% of the total emission).

4 | CONCLUSIONS

Previous studies have identified several important features of scalar transport within vegetated topography, with the most important ones being: (i) the spatial heterogeneity of fluxes out of the canopy even in the presence of uniform scalar sources within the canopy (Katul et al., 2006; Ross, 2011; Ross and Harman, 2015) and (ii) the increased efficiency of out-of-canopy scalar transport in comparison to flat terrain (Ross, 2011). In this work, large eddy simulations of flow over periodic sinusoidal hills covered by dense vegetation were used to investigate the transport of air parcels inside the canopy. By tracking the motion of Lagrangian parcels, we were able to explain the differences between gas transport within forests over flat and complex terrain.

Results show the existence of two main pathways for parcels to be transported out of the canopy. The "local pathway" corresponding to nearly vertical transport out of the canopy by ejection events (with some lateral displacement associated with mean flow advection), and the "advection pathway" corresponding to parcels that travel horizontally towards the recirculation zone in the lee of the hill and sit at the separation point until they are transported out of the canopy by turbulence. The former is the only pathway for canopies over flat terrain. In the presence of topography, both pathways exist as evidenced by the bimodal PDFs of parcel escape location. The dominance of one pathway over the other is determined by the relative time scales for vertical transport by turbulence and mean-wind advection. For the cases studied here, this dominance is determined mostly by depth of release within the canopy, with the local pathway being dominant in the upper canopy and the advection pathway being dominant in the lower canopy.

A major consequence of the advection pathway is that almost all source locations contribute air parcels to the total escape at the separation point, resulting in the "chimney" effect. Sources near the ground will contribute more than sources in the upper canopy, but the collection of parcels from all source locations leads to large total escape at the separation point. This results in the PDFs of escape locations displaying a strong peak at the separation point,

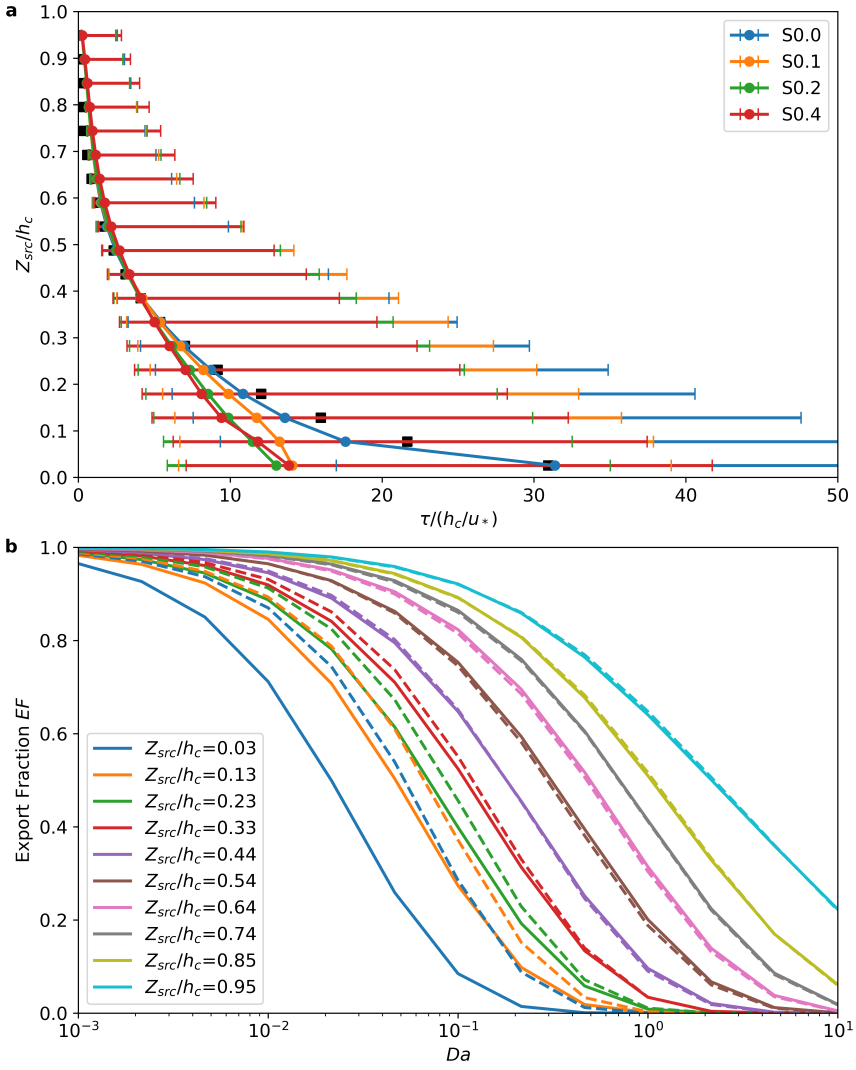

FIGURE 8 (a) Median in-canopy residence times for air parcels released at different heights from the ground. Errorbars indicate 10th and 90th percentiles. The black squares mark the median values obtained from the theoretical model proposed by Gerken et al. (2017) for flat terrain and is shown as reference only. (b) Export fraction of reactive gases as a function of Damköhler number $Da = h_c/(u_*\tau_{\text{chem}})$ for simulations S0.0 (solid lines) and S0.2 (dashed lines). For reference, the value $(h_c/u_*) = 97.5$ s was used in all normalizations, and $\tau/(h_c/u*) = 10$ in (a) corresponds to $\tau \approx 16.3$ min for the present simulations.

which explains the observations of elevated concentrations and fluxes (Katul et al., 2006; Ross, 2011; Ross and Harman, 2015). One important consequence of our findings is that the canopy "volume" footprint for fluxes measured near the separation point is much larger than anywhere else. For gases emitted near the ground, the footprint in this idealized topography is actually the entire domain. Moving forward, it is important to assess these effects in realistic (more complex) topography. If the results observed for periodic sinusoidal ridges hold for realistic topography, interpretation and upscaling of gas fluxes obtained from eddy covariance measurements over complex topography may be more challenging than previously thought.

Vertical transport at the separation point is performed predominantly by turbulence, giving rise to the intermittent accumulation-ejection cycles observed in the flume experiments of Poggi and Katul (2007). However, near the ground where vertical velocity fluctuations are damped, mean vertical advection contributes significantly to transporting air parcels upward to levels of more intense turbulence (where they can be readily transported out of the canopy by ejections). This vertical advection is responsible for a reduction in residence times for gases emitted in the bottom part of the canopy (when compared to flat terrain conditions), which in turn result in a larger escape fraction for reactive compounds. Thus, we conclude that the increased out-of-canopy transport efficiency observed over topography (Ross, 2011) is caused by the small but important effect of mean vertical advection near the ground in the vicinity of the separation point.

Despite the complexity of the flow field and parcel transport studied here, we can envision a path forward towards reduced complexity models of this phenomenon. The leading order effects of the competition between local and advection pathways can be represented by the turbulence intensity $\sigma_w/\overline{u}$. At least for gentle topographies, the existing theoretical framework (Finnigan and Belcher, 2004; Ross and Vosper, 2005; Poggi et al., 2008) can deliver reasonable predictions of the mean velocity field. The applicability of the moving equilibrium hypothesis (Yaglom, 1979) to dense canopies over topography, confirmed by LES runs here, suggest that a parameterization of the vertical velocity variance may be possible from the local stress. In particular, the LES results show that vertical velocity variance profiles inside the canopy across the topography are similar to their flat terrain counterpart. Consequently, it is possible to separate longitudinal variability in the stress above the canopy from the quasi-one dimensional vertical variability in the flow statistics within the canopy. Once the stress at the canopy top is predicted from two-dimensional simplified models, one-dimensional turbulent statistics inside canopies can be reasonably described from second-order closure models using numerical schemes (Meyers and Tha Paw U, 1986; Katul and Chang, 1999; Ayotte et al., 1999; Poggi et al., 2004; Juang et al., 2008) or analytical models (Massman and Weil, 1999). This scale separation framework was already employed to model seed dispersal kernels over complex terrain covered by uniform canopies (Trakhtenbrot et al., 2014).

ACKNOWLEDGEMENTS

This work was supported by the National Science Foundation (NSF-AGS-1644375 to UCLA and NSF-AGS-1644382 to Duke University).

SUPPORTING INFORMATION

The following supporting information is available as part of the online article:
Video S1. Visualization of air parcel trajectories from two sources inside the canopy.

REFERENCES

Ayotte, K. W., Finnigan, J. J. and Raupach, M. R. (1999) A second-order closure for neutrally stratified vegetative canopy flows. *Boundary-Layer Meteorology*, **90**, 189–216.

Bailey, B. N. (2016) Numerical considerations for lagrangian stochastic dispersion models: Eliminating rogue trajectories, and the importance of numerical accuracy. *Boundary-Layer Meteorology*, **162**, 43–70.

Baldocchi, D., Falge, E., Gu, L., Olson, R., Hollinger, D., Running, S., Anthoni, P., Bernhofer, C., Davis, K., Evans, R. et al. (2001) Fluxnet: A new tool to study the temporal and spatial variability of ecosystem-scale carbon dioxide, water vapor, and energy flux densities. *Bulletin of the American Meteorological Society*, **82**, 2415–2434.

Belcher, S. E., Harman, I. N. and Finnigan, J. J. (2012) The wind in the willows: Flows in forest canopies in complex terrain. *Annual Review of Fluid Mechanics*, **44**, 479–504.

Bou-Zeid, E., Meneveau, C. and Parlange, M. (2005) A scale-dependent Lagrangian dynamic model for large eddy simulation of complex turbulent flows. *Physics of Fluids*, **17**, 025105.

Cassiani, M., Katul, G. and Albertson, J. (2008) The effects of canopy leaf area index on airflow across forest edges: large-eddy simulation and analytical results. *Boundary-layer meteorology*, **126**, 433–460.

Chester, S., Meneveau, C. and Parlange, M. B. (2007) Modeling turbulent flow over fractal trees with renormalized numerical simulation. *Journal of Computational Physics*, **225**, 427–448. URL: `http://dx.doi.org/10.1016/j.jcp.2006.12.009`.

Dupont, S., Brunet, Y. and Finnigan, J. J. (2008) Large-eddy simulation of turbulent flow over a forested hill: Validation and coherent structure identification. *Quarterly Journal of the Royal Meteorological Society*, **134**, 1911–1929.

Finnigan, J. J. and Belcher, S. E. (2004) Flow over a hill covered with a plant canopy. *Quarterly Journal of the Royal Meteorological Society*, **130**, 1–29.

Fuentes, J. D., Chamecki, M., dos Santos, R. M. N., Randow, C. V., Stoy, P. C., Katul, G., Fitzjarrald, D., Manzi, A., Gerken, T., Trowbridge, A., Freire, L. S., Ruiz-Plancarte, J., Maia, J. M. F., Tóta, J., Dias, N., Fisch, G., Schumacher, C., Acevedo, O., Mercer, J. R. and Yañez-Serrano, A. M. (2016) Linking meteorology, turbulence, and air chemistry in the amazon rain forest. *Bulletin of the American Meteorological Society*, **97**, 2329–2342.

Gerken, T., Chamecki, M. and Fuentes, J. D. (2017) Air-parcel residence times within forest canopies. *Boundary-Layer Meteorology*, **165**, 29–54.

Grant, E. R., Ross, A. N., Gardiner, B. A. and Mobbs, S. D. (2015) Field observations of canopy flows over complex terrain. *Boundary-Layer Meteorology*, **156**, 231–251.

Hunt, J. C. R., Leibovich, S. and Richards, K. J. (1988) Turbulent shear flows over low hills. *Quarterly Journal of the Royal Meteorological Society*, **114**, 1435–1470.

Juang, J.-Y., Katul, G. G., Siqueira, M. B., Stoy, P. C. and McCarthy, H. R. (2008) Investigating a hierarchy of Eulerian closure models for scalar transfer inside forested canopies. *Boundary-Layer Meteorology*, **128**, 1–32.

Kanani-Sühring, F. and Raasch, S. (2014) Spatial variability of scalar concentrations and fluxes downstream of a clearing-to-forest transition: A large-eddy simulation study. *Boundary-Layer Meteorology*, **155**, 1–27.

Katul, G., Finnigan, J., Poggi, D., Leuning, R. and Belcher, S. (2006) The influence of hilly terrain on canopy-atmosphere carbon dioxide exchange. *Boundary-Layer Meteorology*, **118**, 189–216.

Katul, G., Hsieh, C.-I., Bowling, D., Clark, K., Shurpali, N., Turnipseed, A., Albertson, J., Tu, K., Hollinger, D., Evans, B. et al. (1999) Spatial variability of turbulent fluxes in the roughness sublayer of an even-aged pine forest. *Boundary-Layer Meteorology*, **93**, 1–28.

Katul, G. and Poggi, D. (2010) The influence of hilly terrain on aerosol-sized particle deposition into forested canopies. *Boundary-layer meteorology*, **135**, 67–88.

— (2012) The effects of gentle topographic variation on dispersal kernels of inertial particles. *Geophysical Research Letters*, **39**.

Katul, G. G. and Chang, W.-h. (1999) Principal length scales in second-order closure models for canopy turbulence. *Journal of Applied Meteorology*, **38**, 1631–1643.

Katul, G. G., Mahrt, L., Poggi, D. and Sanz, C. (2004) One-and two-equation models for canopy turbulence. *Boundary-Layer Meteorology*, **113**, 81–109.

Li, Q., Bou-Zeid, E. and Anderson, W. (2016) The impact and treatment of the gibbs phenomenon in immersed boundary method simulations of momentum and scalar transport. *Journal of Computational Physics*, **310**, 237–251.

Lilly, D. K. (1967) The representation of small scale turbulence in numerical simulation experiments. In *IBM Scientific Computing Symposium on environmental sciences*, 195–210. Yorktown heights.

Lin, X., Chamecki, M., Katul, G. and Yu, X. (2018) Effects of leaf area index and density on ultrafine particle deposition onto forest canopies: A LES study. *Atmospheric Environment*, **189**, 153–163.

Liu, Z., Ishihara, T., He, X. and Niu, H. (2016) Les study on the turbulent flow fields over complex terrain covered by vegetation canopy. *Journal of Wind Engineering and Industrial Aerodynamics*, **155**, 60–73.

Massman, W. and Weil, J. (1999) An analytical one-dimensional second-order closure model of turbulence statistics and the lagrangian time scale within and above plant canopies of arbitrary structure. *Boundary-Layer Meteorology*, **91**, 81–107.

Meyers, T. and Tha Paw U, K. (1986) Testing of a higher-order closure model for modeling airflow within and above plant canopies. *Boundary-Layer Meteorology*, **37**, 297–311.

Mittal, R. and Iaccarino, G. (2005) Immerse boundary methods. *Annual Review of Fluid Mechanics*, **37**, 239–261.

Pan, Y., Chamecki, M. and Isard, S. A. (2014) Large-eddy simulation of turbulence and particle dispersion inside the canopy roughness sublayer. *Journal of Fluid Mechanics*, **753**, 499–534.

Pan, Y., Chamecki, M., Isard, S. A. and Nepf, H. M. (2015) Dispersion of particles released at the leading edge of a crop canopy. *Agricultural and Forest Meteorology*, **211-212**, 37–47.

Patton, E. G. and Katul, G. G. (2009) Turbulent pressure and velocity perturbations induced by gentle hills covered with sparse and dense canopies. *Boundary-Layer Meteorology*, **133**, 189–217.

Peskin, C. S. (1972) Flow patterns around heart valves: A numerical method. *Journal of Computational Physics*, **10**, 252–271.

Poggi, D., Katul, G. and Albertson, J. (2004) Momentum transfer and turbulent kinetic energy budgets within a dense model canopy. *Boundary-Layer Meteorology*, **111**, 589–614.

Poggi, D., Katul, G., Albertson, J. and Ridolfi, L. (2007) An experimental investigation of turbulent flows over a hilly surface. *Physics of Fluids*, **19**, 036601.

Poggi, D. and Katul, G. G. (2007) Turbulent flows on forested hilly terrain: the recirculation region. *Quarterly Journal of the Royal Meteorological Society*, **133**, 1027–1039.

— (2008) Turbulent intensities and velocity spectra for bare and forested gentle hills: flume experiments. *Boundary-Layer Meteorology*, **129**, 25–46.

Poggi, D., Katul, G. G., Finnigan, J. J. and Belcher, S. E. (2008) Analytical models for the mean flow inside dense canopies on gentle hilly terrain. *Quarterly Journal of the Royal Meteorological Society*, **134**, 1095–1112.

Queck, R., Bienert, A., Maas, H.-G., Harmansa, S., Goldberg, V. and Bernhofer, C. (2011) Wind fields in heterogeneous conifer canopies: parameterisation of momentum absorption using high-resolution 3d vegetation scans. *European Journal of Forest Research*, **131**, 165–176.

Ross, A. and Vosper, S. (2005) Neutral turbulent flow over forested hills. *Quarterly Journal of the Royal Meteorological Society*, **131**, 1841–1862.

Ross, A. N. (2011) Scalar transport over forested hills. *Boundary-Layer Meteorology*, **141**, 179–199.

Ross, A. N. and Harman, I. N. (2015) The impact of source distribution on scalar transport over forested hills. *Boundary-Layer Meteorology*, **156**, 211–230.

Shaw, R. H. and Schumann, U. (1992) Large-eddy simulation of turbulent flow above and within a forest. *Boundary-Layer Meteorology*, **61**, 47–64.

Shaw, R. H. and Zhang, X. J. (1992) Evidence of pressure-forced turbulent flow in a forest. *Boundary-Layer Meteorology*, **58**, 273–288.

Smagorinsky, J. (1963) General circulation experiments with the primitive equations: I. the basic experiment*. *Monthly weather review*, **91**, 99–164.

Sogachev, A., Leclerc, M. Y., Zhang, G., Üllar Rannik and Vesala, T. (2008) CO2 fluxes near a forest edge: a numerical study. *Ecological Applications*, **18**, 1454–1469.

Tóta, J., Fitzjarrald, D. R. and da Silva Dias, M. A. F. (2012) Amazon rainforest exchange of carbon and subcanopy air flow: Manaus LBA site—a complex terrain condition. *The Scientific World Journal*, **2012**, 1–19.

Trakhtenbrot, A., Katul, G. and Nathan, R. (2014) Mechanistic modeling of seed dispersal by wind over hilly terrain. *Ecological Modelling*, **274**, 29–40.

Wang, W. and Rotach, M. W. (2010) Flux footprints over an undulating surface. *Boundary-Layer Meteorology*, **136**, 325–340.

Wang, W. and Yi, C. (2012) A new nonlinear analytical model for canopy flow over a forested hill. *Theoretical and applied climatology*, **109**, 549–563.

Weil, J. C., Sullivan, P. P. and Moeng, C.-H. (2004) The use of large-eddy simulations in lagrangian particle dispersion models. *Journal of the Atmospheric Sciences*, **61**, 2877–2887.

Wilson, J. D., Finnigan, J. J. and Raupach, M. R. (1998) A first-order closure for diturbed plant-canopy flows, and its application to winds in a canopy on a ridge. *Quarterly Journal of the Royal Meteorological Society*, **124**, 705–732.

Wood, N. (1995) The onset of separation in neutral, turbulent flow over hills. *Boundary-Layer Meteorology*, **76**, 137–164.

Xu, X. and Yi, C. (2013) The influence of geometry on recirculation and CO2 transport over forested hills. *Meteorology and Atmospheric Physics*, **119**, 187–196.

Yaglom, A. (1979) Similarity laws for constant-pressure and pressure-gradient turbulent wall flows. *Annual Review of Fluid Mechanics*, **11**, 505–540.